Astron. Astrophys. 354, 714–724 (2000)

ASTRONOMY AND ASTROPHYSICS

H_α-line impact polarisation by electron beams in solar flares

V.V. Zharkova[1] **and D.V. Syniavskii**[2]

[1] Department of Physics and Astronomy, University of Glasgow, Glasgow G12 8QQ, Scotland, UK
[2] Physics Department, Kiev University, Kiev, 252022, Ukraine

Received 2 June 1998 / Accepted 16 December 1999

Abstract. The H_α-line intensity, linear and circular impact polarisation were calculated during the impulsive phase of flares using the density matrix approach. Depolarising effects of diffusive radiation and collisions with thermal electrons are considered for a 3 levels Hydrogen model atom with Zeeman splitting in weak and intermediate magnetic fields. Electron beam energy and angular distributions in depth are found from the time-dependent anisotropic kinetic solutions in presence of the induced electric field of return current and converging magnetic field. The circular H_α-line polarisation is found to be negligible. The H_α-line profiles of linear polarisation are shown to be affected by electron beams in the line cores whereas wings are fully depolarised by thermal electrons. The full H_α-line linear polarisation, caused by weak or moderate electron beams, is shown to be $2-20\%$ and either positive or negative depending on time after the beam onset and on depth in the atmosphere. The plane of polarisation in the H_α-line is normally perpendicular to the direction of electron beam propagation. Depending on a viewing angle it can be either parallel or perpendicular to the flare-to-solar centre direction. The simulations are used to explain some observational features of the H_α-line polarisation.

Key words: line: formation – plasmas – polarization – Sun: flares

1. Introduction

Observations of the linear polarisation of spectral lines in solar flares provide unique information on the modes of energy transport from the corona to deeper layers during these dynamic events. The H_α-line is the emission most frequently observed in solar flares, and significant properties of the energy transfer process can be derived from measurements of its polarisation vector.

Many H_α-line observations reported an existance of linear polarisation with a degree of polarisation normally in the range of $3-5\%$, in some cases exceeding 10% (Chambe & Hénoux 1979; Hénoux & Semel 1981; Hénoux & Chambe 1990a; Hénoux 1991; Firstova & Boulatov 1996). In most cases the highest degree of polarisation does not correspond to the brightest areas of flares. In the observations by Hénoux et al. (1990b) the direction of plane of polarisation coincides with the flare-to-disk centre direction, whereas some observations by Firstova & Bulatov (1996) show the plane of polarisation to be perpendicular to this direction.

The first interpretation of H_α-line polarisation was made in the approximation of optically thin plasma, using the Born cross-sections for line excitation by charged particles or external radiation (Hénoux & Semel 1981). The observed polarisation was assigned to impact polarisation or to polarisation by high energy radiation (UV and EUV) as the Zeeman or Stark effects produce a polarisation degree of about 0.5% (Hénoux & Semel 1981; Chambe & Hénoux 1979). The authors have also shown that highly energetic particles (electron or protons) produce negative polarisation with the plane of polarisation being mainly perpendicular to the solar centre direction. On the other hand, a directed heat flux can produce positive polarisation with the plane of polarisation being parallel to the solar centre.

In order to explain observed positive polarisation in the H_α-line, low energy proton beams ($E \leq 200$ keV) were used as the source of slow directed fluxes (Hénoux & Chambe 1990a; Hénoux et al. 1993). Their simulations gave a reasonable degree of polarisation. However, they did not take into account the collective effects of proton beams on the ambient plasma which can excite kinetic Alfven waves simultaneously with the H_α-line emission (Voitenko 1998).

Recently, simulations of impact polarisation in H_α-line emission were performed for proton beams precipitating into a flaring atmosphere and causing a redistribution in population between the Zeeman excited states using the density matrix formalism (Vogt et al. 1997). The collisional mechanisms by proton beams and by the ambient plasma electrons, as well as the radiative ones were taken into account for incident and diffusive fields in H_α, L_α and L_β lines. The calculated H_α-line polarisation was found to be lower by up to an order of magnitude than the ones observed during a flare. The simulations only fit observations for a very weak emission at the very beginning of a flare onset although the best fit is found for the quiet Sun or plage models (Vogt et al. 1997). Therefore, in order to get a better fit of polarimetric observations in flares other agents producing H_α- line polarisation should be considered.

Send offprint requests to: V.V. Zharkova, (valja@astro.gla.ac.uk)

As such agents, electron beams were suggested for propagation in the fully ionised plasma of solar flares (Fletcher & Brown 1995). Their simulations gave a degree of polarisation of about $5-7\%$, but required electron beams with very high initial energy fluxes of $10^{13}-10^{15} erg \cdot cm^{-2} \cdot s^{-1}$. They are three orders of magnitude higher than typical fluxes deduced from the X-ray observations in solar flares.

In many flares the H_α-line emission is very bright and wide, so it is likely to be optically thick. Moreover, at chromospheric depths, where magnetic field can reach 1000 Gs (Lozitskii & Baranovskii 1993; Silva et al. 1996), the hydrogen atom levels are likely to be split. Therefore, for the interpretation of H_α-line polarisation it is necessary to include these two effects. This can be done using the density matrix approach. It has been applied earlier to the HeD_3 line in solar prominences (Bommier 1980; Landi Degl'Innocenti 1982) and for Hydrogen lines in flares (Vogt et al. 1997). Recently, the transfer of polarised radiation of two-level hydrogen atoms embedded in an optically thick magnetised medium was generalised for weak, intermediate and strong magnetic fields (Landi Degl'Innocenti et al. 1990, 1991b; Bommier et al. 1991; Bommier et al. 1996; Landi Degl'Innocenti 1996).

In the present paper, the effect of electron beam injection on the H_α-line polarisation during the impulsive phase of flares is investigated in a magnetised plasma loop using the approach similar to those of Vogt et al. (1997). Firstly, the solutions of the time-dependent Boltzman equation were used for beam electrons with anisotropic scattering in presence of the return current electric and converging magnetic field (Zharkova et al. 1995). Secondly, the diffusive H_α radiation field for a 5 level hydrogen model atom without fine structure was calculated in the full non-LTE approach as described by Zharkova & Kobylinsky (1989, 1991, 1993). And, thirdly, the density matrix technique was applied for the solution of a steady state equation in a flaring atmosphere with angular anisotropy caused by electron beam impacts and external radiation by the method of Landi Degl'Innocenti (1985).

2. Basic models

2.1. Physical model

An elementary magnetic flux tube filled by an hydrogenic plasma is considered to be affected by electron beam injection. The beam causes a hydrodynamic response of the ambient plasma calculated using the hydrodynamic models by Somov et al. (1981), developed by Zharkova & Brown (1995). The newer HD models have been calculated by Mariska et al. (1989), Li et al. (1989) and others. However, all these models have the differences which only occur at the upper coronal and chromospheric levels but do not affect the lower chromospheric levels. This allows to use the HD models by Somov et al. (1981) with temperature, density and macrovelocity variations in time and depth as shown in Fig. 1 in the paper by Zharkova & Kobylinsky (1993).

The main features of such a response can be briefly described as follows. The beam injection produces a strong downward shift of the transition region into deep atmospheric levels which, in turn, causes a sharp increase in temperature and a decrease in total density at the coronal levels. This is followed by evaporation of the chromospheric plasma into the corona and by formation of a dense cold condensation in the chromosphere which moves downwards to the photosphere as a shock wave. This paper deals with the chromospheric part of the HD simulations above, namely, with the cold and dense condensation in which the H_α-line emission originates. The HD models for temperature, density, macrovelocity were calculated for the first 10 sec after an electron beam onset.

2.2. Kinetic model

Electron beams are considered to be injected from the corona into a flaring atmosphere along the magnetic field direction with normal distributions in pitch-angles and time. In order to find an electron population at each depth, the time-dependent Boltzman equation was solved numerically for beam electrons with energy power law and normal distributions in pitch-angles and time, precipitating from the corona into deeper atmosphere in presence of the induced electric field of return current and converging magnetic field (Zharkova et al. 1995). The beam electrons are assumed to lose their energy in collisions with charged particles and neutral hydrogen atoms, in Ohmic heating and anisotropic scattering. While solving the kinetic equation in the phase space of time, depth, energy and pitch angle, the time and depth variables are considered to be independent whereas the energy and pitch-angle variables are to be dependent on the first two as they vary with depth and time (Emslie 1980). This, in turn, results in additional boundary conditions being imposed on the energy and pitch-angle dependence on depth and time (see for details Zharkova et al. 1995).

Some results of the simulations are shown in the paper by Zharkova et al. (1995) (Figs. 1 and 2) for the following beam parameters: the lower energy cutoff was equal to 15 keV, electron beam spectral index $\gamma = 3$ and initial energy flux $F_0 = 2 \cdot 10^{11}$, upper energy cutoff $E_2 = 250 keV$ (Fig. 1) and $\gamma = 6$, $F_0 = 2 \cdot 10^9$, $E_2 = 150 keV$ (Fig. 2). For the upper energy cutoff ≥ 150keV, moderate spectral indices and initial fluxes on the top boundary, electron beams were shown to reach lower chromospheric and even photospheric levels as collimated beams with power law in energy, despite the disruptive effects of a return current at the transition region level and in the upper chromosphere.

There are significant variations in the energy loss mechanisms throughout this precipitation. At upper levels in the corona, where the ambient plasma is fully ionised, Coulomb collisions dominate the other energy losses; at the transition region and upper chromosphere, these are comparable with Ohmic losses, with the latter causing a disruption of the initial beam and the appearance of a 'return current beam', returning to the source in the corona. This, in turn, produces a split in energy of the initial beam with the additional maximum at 30-35 keV.

In the lower chromosphere, where the ambient plasma is weakly ionised with ionisation degree of 10^{-4} (Zharkova &

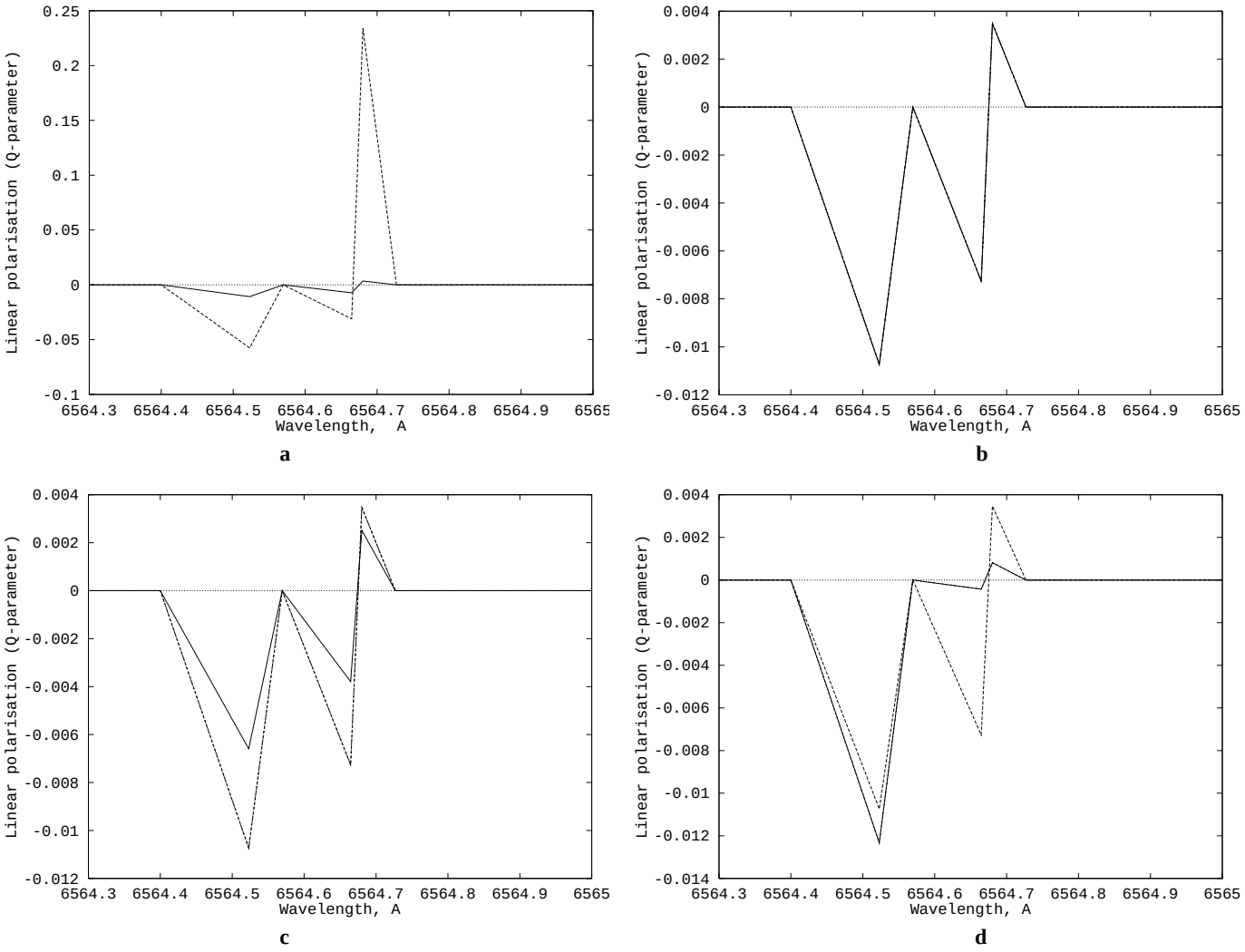

Fig. 1a–c. The H_α-line polarisation profiles (linear polarisation - parameter Q) plotted for the depths **a** - $1.37 - 2.78 \cdot 10^{20} cm^{-2}$, **b** - $4.96 - 7.36 \cdot 10^{20} cm^{-2}$, **c** - $8.50 - 9.76 \cdot 10^{20} cm^{-2}$ and **d** - $1.21 - 2.52 \cdot 10^{21} cm^{-2}$ for for a viewing angle $\theta = \pi/2$, at the moment t= 4.39 s for beam parameters: solid line - spectral index $\delta = 4$, dashed line - $\delta = 7$; $F_0 = 210^9 erg/cm^2/s$

Kobylinskii 1989), inelastic collisions of beam electrons with neutral atoms prevail over any other energy losses. Since the cross-sections of such collisions are much lower than those of Coulomb collisions, beam electrons lose less their energy in these collisions and can precipitate downward to the photosphere, despite an increase in the total density. Electron beams, which are well directed along the magnetic field, still precipitate as collimated beams to the lower atmospheric levels, but they are transformed into softer beams with wider angular distributions (Zharkova et al. 1995).

The part of beam electrons which reaches the lower chromosphere can produce a dual effect on the atmosphere: first, the formation from the hydrodynamic response of a cold dense condensation, as described in Sect. 2.1; and, secondly, additional excitation, ionisation and polarisation of Hydrogen atoms by inelastic collisions, as considered below in Sect. 2.3.

2.3. Radiative model

For polarimetric simulations a 3 level Hydrogen model atom (total 9 sublevels: $1s_{1/2}, 2s_{1/2}, 2p_{1/2}$, $2p_{3/2}, 3s_{1/2}, 3p_{1/2}, 3p_{3/2}$, $3d_{3/2}$ and $3d_{5/2}$) was considered with fine structure of the third and second levels caused by Zeeman splitting without level crossings. Only Zeeman coherence, like $\langle nLJM|\rho|nLJM'\rangle$, will be taken into account whereas all other coherences with $n' = n$, $L' = L$ and $J' = J$ can be omitted following the estimation $\Gamma \ll \frac{\Delta E_{FS}}{\hbar}$, where $\Gamma \propto xB$ is the atomic energy of the Bohr frequency set, B is the magnetic induction in G; x is about unity; ΔE_{FS} is the energy splitting from the spin-orbital interaction.

Steady state equations were solved for all these transitions (104 in total) using the density matrix with both collisional (thermal and non-thermal) and radiative tensors. Radiative transfer equations were not directly included into this solution because the opacities evaluated in the H_α-line fine structure transitions

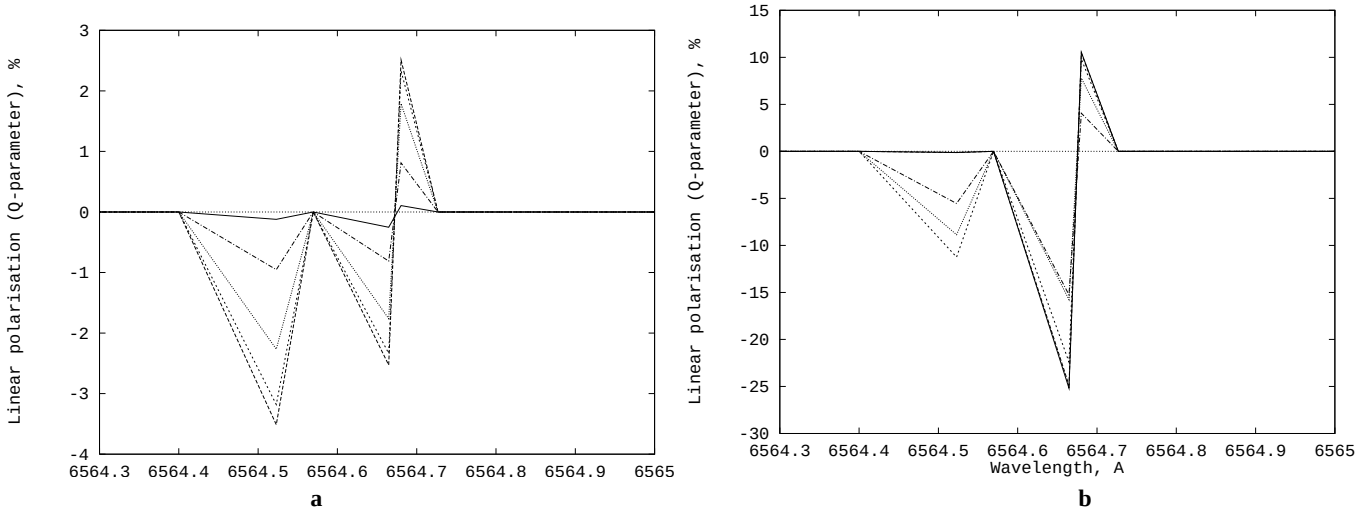

Fig. 2a and b. The H_α-line polarisation profiles (linear polarisation - parameter Q) plotted for the depth $\xi = 7.36 \cdot 10^{20} cm^{-2}$, at the moments t= 2.92s (a) and t= 5.94s (b) for 5 viewing angles $\theta = (0.1, 0.2, 0.3, 0.4, 0.5)\pi$ (from the top to the bottom in each subfigure, respectively). The peaks are correspondent to the allowed transitions as in the text; beam parameters are correspondent to the softer beam from Fig. 1.

were appeared to be lower than unity in most cases, whereas their integrated opacity was well above unity. Therefore, the full radiative transfer problem solution can be omitted for these transitions by replacing it with an averaged radiative transfer solution applied to the H_α-transitions without the fine structure. This approach for H_α-line can be supported by conclusions of Bommier et al. (1991) where the radiative transfer problem was solved for a 3 level hydrogen atom with fine structure in optically thick media.

In order to calculate a diffusive mean intensity and a degree of ionisation in these dynamic events, we used a 5 levels plus continuum model atom without fine structure. The full non-LTE approach was applied for all the transitions at different depths and times, as described by Zharkova & Kobylinsky (1989, 1993) and Kobylinskii & Zharkova (1996). Collisions with thermal and beam electrons were considered along with radiative excitation/ionisation and deactivation by the external radiation in all the transitions considered.

The ionisation balance in a flaring atmosphere was found to be governed by Hydrogen atom ionisation. In the lower chromosphere, if thermal electrons only are considered, the hydrogen ionisation degree falls sharply down to a magnitude of 10^{-4}. Beam electrons reaching this depth mostly ($90 - 95\%$) lose their energy in inelastic collisions with neutral Hydrogen atoms (Aboudarham & Hénoux 1986, 1987; Zharkova & Kobylinsky 1989). These collisions increase the Hydrogen ionisation degree to about 10^{-2} (see Fig. 2 in Zharkova & Kobylinsky (1989). This, in turn, causes an enhancement in Lyman, Balmer, Pashen line wings and heads of continua.

2.3.1. Evaluation of elementary processes

Hydrogen atoms, embedded into a flaring atmosphere of a magnetic flux tube, are affected by depolarising collisions with thermal electrons of the ambient plasma and by polarising collisions with anisotropic beam electrons and external radiation. As the atom levels in a magnetic field are split into sublevels of the fine structure, it is important to evaluate the effect of each mechanism.

1. *Magnetic field effect* According to Bommier & Landi Degl'Innocenti (1996), a weak magnetic field can partially destroy the coherence between magnetic sublevels, whereas Zeeman splitting should still not be taken into account (effect Hanle). In this case the following condition is valid:

$$\nu_L = A, \tag{1}$$

where ν_L is the Larmor frequency and A is the Einstein spontaneous emission rate.
In the case of an 'intermediate' magnetic field the coherence between magnetic sublevels is absent and in comparison with the Doppler width, Zeeman splitting is noticeable. In this case the condition above can be rewritten as:

$$A \ll \nu_L < \Delta\nu_D, \tag{2}$$

here $\Delta\nu_D$ is the Doppler width.
The temperature in the model flaring atmospheres from Sect. 2.1 lies in a range of $10^4 - 6 \cdot 10^3$ ^{o}K which results in $\Delta\nu_D \approx 10^{12} - 10^{10} s^{-1}$. Magnetic field in the chromosphere can vary from 500 to 1500 G (Lozitskii & Baranovskii 1993; Silva et al. 1996), so $\nu_L = (3-20) \cdot 10^8 s^{-1}$. Therefore, in the chromosphere, where the H_α emission originates, these two regimes may occur and both should be considered. It should also be noted that in the line formation region Hanle effect will prevail in the line core, whereas in the wings the 'intermediate' magnetic field approximation is valid.
2. *Effects of collisions and radiation anisotropy*
Let evaluate a role of depolarising collisions with thermal electrons and of an anisotropy of incident radiation at

these levels. The anisotropy of the incident radiation is described by the parameter R_a which is determined by the non-diagonal elements of the density matrix. The isotropic part of radiation is described by the parameter R_i which is determined by the diagonal elements. Therefore, spectral line polarisation, caused by anisotropy of radiation, is proportional to the ratio R_a/R_i. The effect of depolarising collisions can be described by the parameter D, which accordingly is proportional to the plasma density N:

$$D = N\sigma V, \tag{3}$$

where σ is a sum of the collisional cross-sections in the H_α-line transitions up and down, V is the relative velocity between atoms and colliding particles. If σ is in units of $10^{-16}cm^2$ and V is in km/s, then:

$$D = N\sigma V \cdot 10^{-11},\ \ s^{-1} \tag{4}$$

Radiation anisotropy R_a can be described by the formulae:

$$R_a = W \cdot B_{lu} \cdot J, \tag{5}$$

where W is the dilution factor of the external chromospheric H_α radiation, varying from 0.3 to 0.5, B_{lu} - the Einstein's absorption coefficient and J - the mean radiation intensity. For a strong optical line with the effective temperature of 6000^o K, $R_a = W \cdot 10^6 s^{-1}$. The condition $D = R_a$ leads to the following evaluation of the critical density where the collisional and radiative probabilities are comparable:

$$N_{crit} = W \cdot (\sigma V)^{-1} \cdot 10^{17},\ \ cm^{-3} \tag{6}$$

Considering $W \cdot (\sigma V)^{-1}$ as being of $10^{-2} - 10^{-3}$, for the temperature range relevant to a flaring atmosphere, the critical density is $N_{crit} = 10^{14} - 10^{15} cm^{-3}$. This corresponds to the temperature minimum region in the quiet atmosphere, while in flares this density can be reached at the lower chromospheric levels where the H_α-line wing emission occurs.

3. Density matrix approach

For a description of the Hydrogen atomic system interacting with an external and diffusive radiation field and particles (thermal and non-thermal electrons), according to Berestetskij et al. (1989), Landi Degl'Innocenti (1983), Bommier & Degl'Innocenti (1996), the density matrix ${}^{nLJ}\rho^A_{MM'}$ was considered where n is the main quantum number, L is the orbital atomic momentum, J is the total atomic momentum, M - the total angular momentum projected on the magnetic field direction, A stands for 'atomic'. The diagonal elements of the density matrix describe the populations of the atomic levels and the non-diagonal elements describe the coherence between two different levels.

As described in Sect. 2.3 a steady state equation for the density matrix with radiation and collisional tensors was solved including all levels of the fine structure above. However, for these levels the radiative transfer equations were not taken into account as their opacity is below unity and the optically thin approach gives a reasonable approximation (Bommier et al. 1991). Instead an averaged diffusive radiation field in the transition $2 \rightarrow 3$ was used from the full non-LTE problem solution for 5 level plus continuum hydrogen atom without fine structure (Zharkova & Kobylinsky 1991). This approach has also been used by other authors (Vogt et al 1997) and gave reliable results.

3.1. Steady state equation

A steady state equation for the density matrix can be written as follows:

$$\begin{aligned}
&\frac{d}{dt}{}^{n_1L_1J_1}\rho^A_{M_1M_1'} = \\
&\frac{i}{\hbar}[E(n_1L_1J_1M_1) - E(n_1L_1J_1M_1{}')]^{n_1L_1J_1}\rho^A_{M_1M_1'} \\
&+ \sum_{\substack{M_2M_2' \\ L_2J_2 \\ n_2}} P^{tot}{}_{n_1L_1J_1M_1M_1' \leftarrow n_2L_2J_2M_2M_2'}{}^{n_2L_2J_2}\rho^A_{M_2M_2'} \\
&- \sum_{\substack{M_2M_2' \\ L_2J_2 \\ n_2}} P^{tot}{}_{n_2L_2J_2M_2M_2' \leftarrow n_1L_1J_1M_1M_1'}{}^{n_1L_1J_1}\rho^A_{M_1M_1'}
\end{aligned} \tag{7}$$

where $P^{tot}_{n_1L_1J_1M_1M_1' \leftarrow n_2L_2J_2M_2M_2'}$ and $P^{tot}_{n_1L_1J_1M_1M_1' \rightarrow n_2L_2J_2M_2M_2'}$ are the total probabilities of the transitions $\langle n_1L_1J_1M_1M_1'|\rho^A|n_2L_2J_2M_2M_2'\rangle$ from and to upper level respectively. These, in turn, are determined by the sum of the probabilities of spontaneous P^{sp}, induced radiation P^{ind}, absorption P^{abs} and collisional transitions P^{coll}, taking into account impacts with both thermal and beam electrons.

The first member of the above equation describes the probability of transitions between sublevels, split in magnetic field, the second member corresponds to the probability of the level excitation and the third - to the probability of its de-excitation.

3.2. Radiative tensor

In order to describe anisotropy of the radiation field, the radiation field tensor for H_α-line frequencies in a solid angle $\Omega = (\chi; \theta)$ in the plane perpendicular to the direction of emitted quanta can be introduced as follows:

$$\overline{\Phi}^{rad}_{ij} = \int \Phi^{rad}_{ij}(\omega) \frac{1}{\sqrt{\pi}} \exp\left[-\left(\frac{\Delta\omega}{\Delta\omega^D{}_{H_\alpha}}\right)^2\right] d\omega, \tag{8}$$

with

$$\Phi^{rad}_{ij}(\omega) = \int \frac{d\Omega}{4\pi} I_\omega(\Omega) f_{ij}(\overrightarrow{\Omega}); \tag{9}$$

where i,j = x, y, z and f_{ij} is the transition matrix from the electron to emitted photon coordinate systems depending on the azimuthal χ and longitudial θ angles.

For the calculation in the H_α-line frequencies a normalised radiative tensor ϕ_{ij}^{rad} is used:

$$\phi_{ij}^{rad} = \frac{\overline{\Phi}_{ij}^{rad}}{\sum_{I=1}^{3} \Phi_{ii}^{rad}}. \quad (10)$$

In Ly_α and Ly_β lines, owing to their big opacity and assumed detailed balance, the radiative tensor has a form:

$$\phi_{ij}^{rad} = \frac{1}{3}\delta_{ij}, \quad (11)$$

where δ_{ij} is the Kronecker function.

The local radiation density can be described as:

$$u^{rad} = \int_{(2\pi)} I_\omega(\Omega) d\overrightarrow{\Omega}. \quad (12)$$

with $I_\omega(\overrightarrow{\Omega})$ being a local intensity in a solid angle Ω found from the non-LTE radiative transfer equation as described in Sect. 2.3.

3.3. Collisional tensor

The collisional tensor describes the radiation anisotropy caused by collisions with both thermal and beam electrons. Thermal electrons have a Maxwellian distribution in energy and their collisional tensor can be written as follows:

$$\phi_{ij}^{coll} = \frac{1}{3}\delta_{ij}, \quad (13)$$

whereas for beam electrons the following expression can be used:

$$\overline{\Phi}_{ij}^{coll} = \int_{(4\pi)} \frac{d\overrightarrow{\Omega}}{4\pi} f_{ij}(\Omega) \int_0^\infty \rho_{beam}(t,\xi,v,\theta) v^2 dv, \quad (14)$$
$$i,j = x,y,z$$

where ρ_{beam} is a normalised dimensionless electron beam distribution function, t - an injection time, ξ is a depth and θ is a pitch-angle. For the calculations a normalised collisional tensor ϕ_{ij}^{coll} was used with the normalisation being similar to the radiative tensor above. Also the local collisional density ccan be introduced as follows:

$$u^{coll} = \int_{(4\pi)} \rho(\overrightarrow{\Omega}) d\overrightarrow{\Omega}, \quad (15)$$

where ρ is a sum of Maxwellian and power law energy distributions for thermal and beam electrons, respectively, that was calculated as described in Sect. 2.2.

3.4. Probabilities of radiative transitions

The probability of spontaneous transition can be described as follows (Bommier 1980):

$$P^{spon}_{n_1L_1J_1M_1M_1' \leftarrow n_2L_2J_2M_2M_2'} =$$
$$D_{n_1L_1J_1M_1M_1' \leftarrow n_2L_2J_2M_2M_2'}(-m,-m') \times$$
$$(2L_2+1) A(n_2L_2S \rightarrow n_1L_1S) \quad (16)$$

where D is a matrix term presented in the form:

$$D_{n_1L_1J_1M_1M_1' \leftarrow n_2L_2J_2M_2M_2'}(-m,-m') =$$
$$\begin{pmatrix} J_1 & 1 & J_2 \\ -M_1 & -m & M_2 \end{pmatrix} \begin{pmatrix} J_1 & 1 & J_2 \\ -M_1' & -m' & M_2' \end{pmatrix} \times$$
$$(2J_1+1)(2J_2+1) \times$$
$$\begin{bmatrix} J_1 & 1 & J_2 \\ L_2 & S & L_1 \end{bmatrix}^2 \quad (17)$$

with $m = M_2 - M_1$; $m' = M_2{}' - M_1$.

For induced radiation, the probability will be:

$$P^{ind}_{n_1L_1J_1M_1M_1' \leftarrow n_2L_2J_2M_2M_2'} =$$
$$D_{n_1L_1J_1M_1M_1' \leftarrow n_2L_2J_2M_2M_2'}(-m,-m') \times$$
$$(2L_2+1) 3u^{rad}\phi^{rad}_{mm'} B(n_2L_2S \rightarrow n_1L_1S) \quad (18)$$

and for absorbed radiation, the probability is equal to:

$$P^{abs}_{n_1L_1J_1M_1M_1' \rightarrow n_2L_2J_2M_2M_2'} =$$
$$D_{n_1L_1J_1M_1M_1' \leftarrow n_2L_2J_2M_2M_2'}(-m,-m') \times$$
$$(2L_2+1) 3u^{rad}\phi^{rad}_{mm'} B(n_2L_2S \leftarrow n_1L_1S) \quad (19)$$

with $A(n_2L_2S \rightarrow n_1L_1S)$, $B(n_2L_2S \rightarrow n_1L_1S)$ and $B(n_2L_2S \leftarrow n_1L_1S)$ being the Einstein coefficients of spontaneous, induced emission and absorption respectively.

3.5. Probabilities of collisional transitions

The probability of the first kind collisional transitions (from lower levels to higher levels) can be written as (Berestetskii et al. 1989):

$$P^{coll}_{n_1L_1J_1M_1M_1' \rightarrow n_2L_2J_2M_2M_2'} =$$
$$D_{n_1L_1J_1M_1M_1' \rightarrow n_2L_2J_2M_2M_2'}(-m,-m') \times$$
$$\sigma_{eff}(n_1L_1S \leftarrow n_2L_2S) u^{coll} \phi^{coll}_{m'm} \quad (20)$$

where D is the matrix determined from formula (17).

For the second kind collisional transitions (from higher to lower levels) the probability is:

$$P^{coll}_{n_1L_1J_1M_1M_1' \leftarrow n_2L_2J_2M_2M_2'} =$$
$$D_{n_1L_1J_1M_1M_1' \leftarrow n_2L_2J_2M_2M_2'}(m,m') \times$$
$$\sigma_{eff}(n_1L_1S \rightarrow n_2L_2S) u^{coll} \phi^{coll}_{mm'} \quad (21)$$

where σ_{eff} is the effective cross-section, which can be determined by the Born formulae. The matrix terms for the transitions from upper to lower level $D(m,m')$ are described by formula (17) above with m and m' having the opposite signs.

3.6. Stokes parameters

The Stokes parameters are linked to the density matrix as follows:

$$S_1 \equiv U = i[\langle \overrightarrow{n}, -1|\rho|\overrightarrow{n}, +1\rangle - \langle \overrightarrow{n}, +1|\rho|\overrightarrow{n}, -1\rangle] \quad (22)$$
$$S_2 \equiv V = [\langle \overrightarrow{n}, +1|\rho|\overrightarrow{n}, +1\rangle - \langle \overrightarrow{n}, -1|\rho|\overrightarrow{n}, -1\rangle] \quad (23)$$
$$S_3 \equiv Q = -[\langle \overrightarrow{n}, -1|\rho|\overrightarrow{n}, +1\rangle + \langle \overrightarrow{n}, +1|\rho|\overrightarrow{n}, -1\rangle]$$

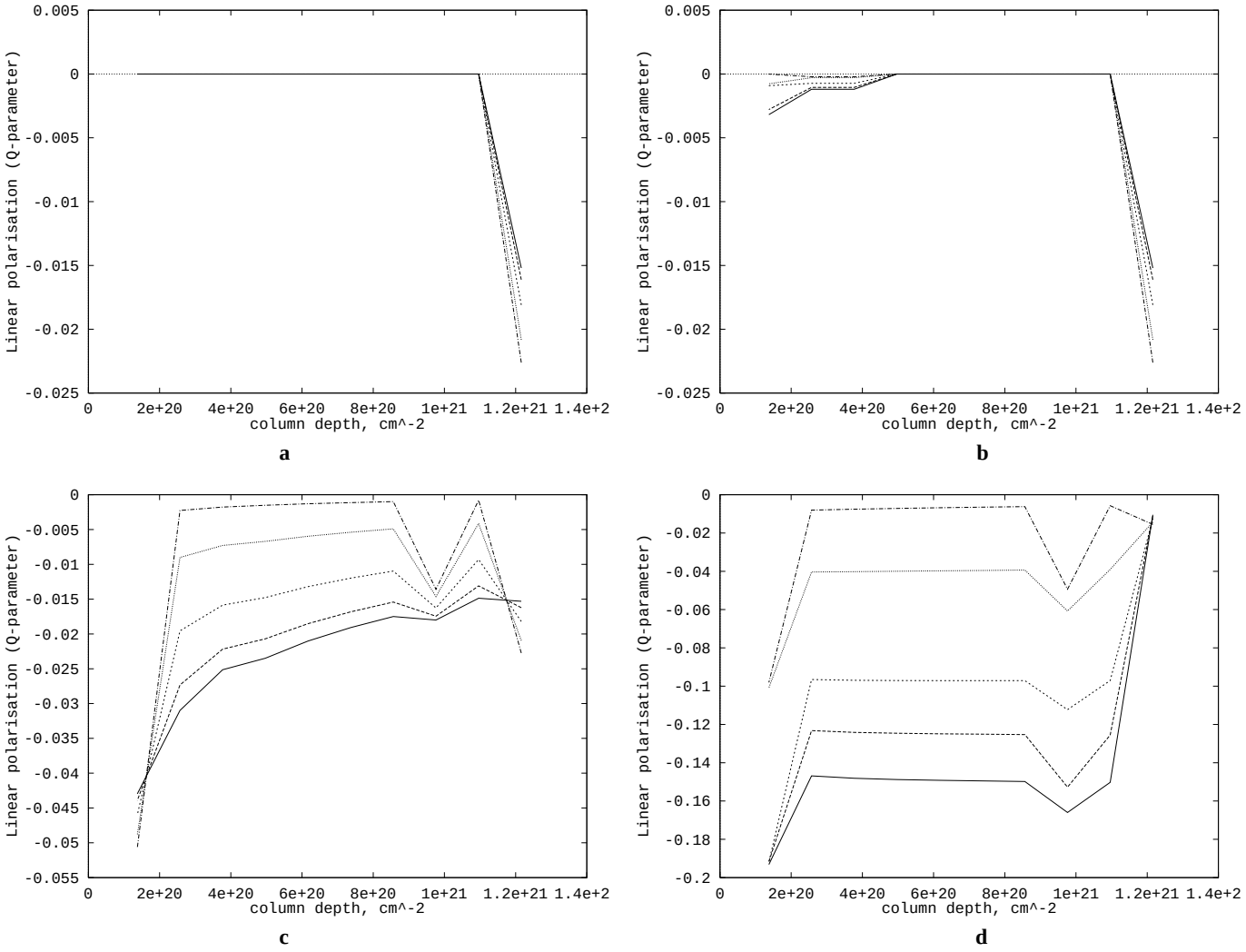

Fig. 3a–c. The H_α-line full polarisation (linear polarisation - parameter Q), plotted versus depth in a flaring atmosphere at the moments t=0.01s (a), t=1.46s (b), t= 2.92s (c) and t= 5.94s (d) for different viewing angles $\theta = (0.1, 0.2, 0.3, 0.4, 0.5)\pi$ (from top to bottom in each subfigure). Beam parameters: $F_0 = 2 \cdot 10^{11} erg/cm^2/s$, $\delta = 5$.

Polarisation is considered in the following two directions: the axis ξ along a magnetic field direction and the axis θ perpendicular to it. A viewing angle in this model coincides with a pitch-angle; the flare-to-solar centre direction deviates from a magnetic field direction on this angle. The parameter S_3 describes linear polarisation along these axes ξ and θ, the value of $S_3 = 1$ corresponds to full polarisation in the direction parallel to magnetic field lines and $S_3 = -1$ - to full polarisation in the perpendicular direction. The parameter S_1 gives linear polarisation in the direction with the angles of $\phi = \pi/4$ or $\phi = -\pi/4$ to the observer's line of sight. The parameter S_2 describes circular polarisation with the probabilities $(1 + S_2)/2$ and $(1 - S_2)/2$ of photon having a left-handed or right-handed polarisation. In astrophysical applications these parameters are defined as: $S_1 \equiv U$, $S_2 \equiv V$ and $S_3 \equiv Q$.

4. Results and discussion

The results of simulations of the H_α-line polarisation are presented in Figs. 1-4. In Fig. 1 the H_α-line linear polarisation profiles are plotted versus wavelengths at t= 4.39 s after an electron beam onset ($F_0 = 2 \cdot 10^9 erg/cm^2/s; \delta = 4, 7$) for viewing angle $\theta = \pi/3$ and different depths. In Fig. 2 the linear polarisation profiles are plotted for different viewing angles and two different times of the beam injection for softer beams ($\delta = 7$). In Fig. 3 and Fig. 4 respectively the full (integrated in wavelength) linear polarisation and intensity caused by soft weak beam above ($\delta = 7$) are plotted versus depth in a flaring atmosphere for viewing angle $\theta = \pi/3$ at different times.

The calculations show that impacts with beam electrons in a flaring atmosphere mainly lead to linear polarisation of the H_α-line emission whilst circular polarisation is negligible. This is in agreement with the most observations (Hénoux & Chambe 1990a; Firstova & Boulatov 1996). It could be understood in

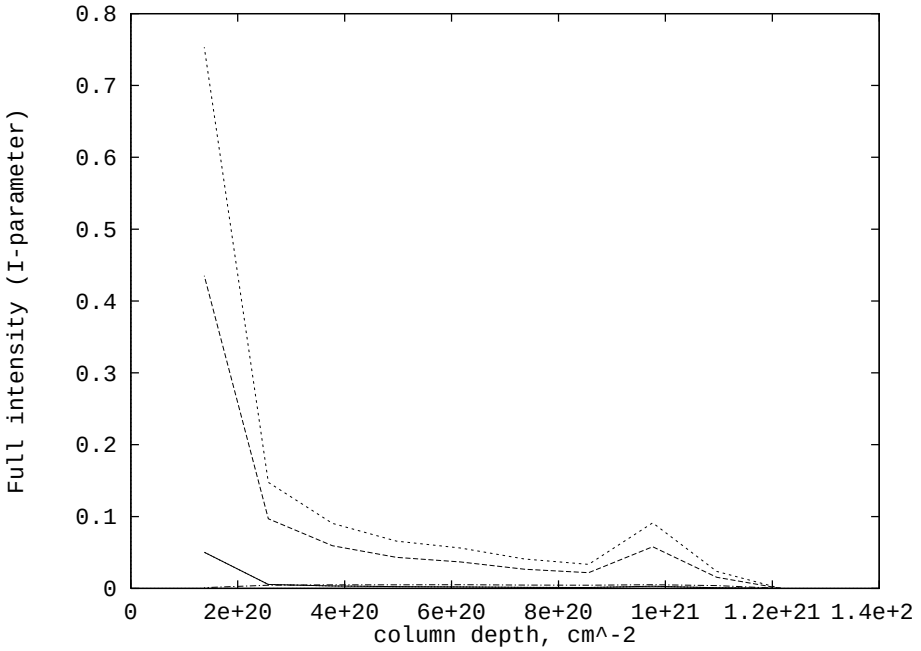

Fig. 4. The H_α-line full intensity (parameter I), plotted versus depth in a flaring atmosphere for different transitions of the fine structure at the moment t= 4.39s (upper curve corresponds to $3d_{5/2} \rightarrow 2p_{3/2}$, then in the descent order: to $3p_{3/2} \rightarrow 2s_{1/2}$ and $3d_{3/2} \rightarrow 2p_{3/2}$. Beam parameters are the same as in Fig. 2.

terms of radiation with circular polarisation to be produced by small angular deviations of higher energy electrons in collisions with the ambient plasma charged particles (Berestetskii et al. 1989). However, as the beam kinetics shows, in the lower chromosphere the number of such electrons is very small, and they can not produce a significant effect.

There is a wide range of absolute values of linear polarisation in the line profile varying from a few tenths of percent (t= 1.46 s, Fig. 1b) to $12-15\%$ (t=4.39 s, Fig. 1d). The maximum ($20-25\%$) of the full H_α-line linear polarisation was found for softer weaker electron beams ($F_0 = 2 \cdot 10^9 erg/cm2/s$, δ= 7) whilst for harder beams the degree of linear polarisation is lower ($5-8\%$).

This behaviour is similar to those of hard X-ray bremsstrahlung polarisation (Zharkova et al. (1995), although the X-ray polarisation is slightly decreased with enhancement of initial flux during the injection whereas the H_α line polarisation steadyly increases with time. This occurs because of a difference in radiative cross-sections for radiation in these ranges: X-ray emission is a direct reproduction of electron beam distributions. However, the H_α quanta are slightly delayed by the line opacity caused by a radiative transfer and Doppler and Stark line broadening effects.

Therefore, at the higher chromosphere and transition region where the return current effect causes a decrease in a number of beam electrons precipitating downwards, it also decreases X-ray emission and polarisation. In the lower chromosphere where the H_α-emission originates, only a residual part of electrons which moved from higher to lower energy distributions can contribute to this emission. The number of these electrons increases with time and depth and their excitation and ionisation rates prevail over the thermal ones. Thus, beam electrons can excite or ionise more and more hydrogen atoms throughout their precipitation. This accumulative effect results in a steady increase of the H_α-line polarisation during the beam injection.

4.1. H_α-line polarisation profiles

Electron beam effects on the H_α-line profiles are rather asymmetric. The profiles are plotted with maximums corresponding to the main transitions with $3d_{3/2}-2p_{1/2}$, and $3p_{3/2}-2s_{1/2}$). In order to demonstrate a pure polarisation effect, all other broadening factors such as Doppler and Stark effects are excluded from these profiles in Figs. 1-2, although the calculations were performed including these effects. As expected, the impact polarisation appears only in line cores whereas wings are fully depolarised by collisions with thermal electrons.

At the initial phase of beam injection, only the blue core ($\leq -0.1A^o$ from the central wavelength) in the H_α-line polarisation profile is affected by impacts with beam electrons, as it is seen in Fig. 2a. This effect varies from -1% for a viewing angle of 0.1π to -3.5% for a viewing angle of 0.5π. With further beam penetration into a flaring atmosphere the polarisation increases up to -12% in the blue core and to -25% in the red core (at $+0.1A^o$ and more from the central wavelength). More powerful soft beams produce higher negative polarisation of about $20-25\%$ at higher depths of $10^{20} cm^{-2}$ decreasing to a few percent at the lower depth of $10^{21} cm^{-2}$ (see Fig. 2b).

At the top depth where $\xi = 1 \cdot 10^{20} cm^{-2}$ radiation from the transitions $3d_{5/2} - 2p_{3/2}$, and $3p_{3/2} - 2s_{1/2}$) have negative polarisation whereas in the transition $3d_{3/2} - 2p_{3/2}$ polarisation is positive reaching 25% (Figs. 1a and 2b) while the beam reaches a maximum energy flux. Positive polarisation shows a small decrease with depth down to $3-5\%$ for a viewing angle of 0.1π and to 10% for a viewing angle of 0.5π. However, its contribution to the integrated polarisation is rather small and the full line polarisation stays negative.

These variations of H_α-line polarisation profiles are believed to reflect a pitch-angular anisotropy of beam electrons at these depths. For radiation in the transitions ($3d_{5/2} - 2p_{3/2}$, and $3p_{3/2} - 2s_{1/2}$)) more energetic beam electrons are required than for the lower energy transition ($3d_{3/2} - 2p_{3/2}$). As the beam kinetics show, some part of the initial electron beam was transformed into a secondary beam with lower energy electrons returning to the corona. These electrons are scattered to pitch-angles between $90 - 180^o$, according to the kinetic solutions by Zharkova et al. (1995).

It produces additional polarisation with the plane of polarisation being perpendicular to the direction of the secondary beam, but parallel the direction of the initial beam. For an observer at these levels it results in positive polarisation in this transition. At lower depths an anisotropic scattering effect decreases and coincides with a decrease of the number of electrons scattered to bigger pitch-angles as it was shown from the kinetics. This leads to a decrease to a few percent in this positive polarisation.

Therefore, full line polarisation will be a sum of polarisation degrees in each of these transitions and is dependent on the number of beam electrons in the initial and secondary beams.

4.2. Depth and time variations of H_α-line polarisation

Beam electron impacts become noticeable in the H_α-line polarisation from a column depth of $\xi = 0.2 \cdot 10^{20} cm^{-2}$ which coincides with those defined from the non-LTE simulations of Hydrogen emission without atomic fine structure (Zharkova & Kobylinskii 1989, 1993).

At lower chromospheric levels, from $\xi = 1.2 \cdot 10^{21} cm^{-2}$, anisotropic external radiation is a dominant mechanism in the H_α-line polarisation producing polarisation of about 2% (Fig. 3a). The mean intensity of this external H_α-radiation is higher by an order of magnitude than those of the diffusive H_α-line emission which is produced in absence of beam electrons.

The effect of beam impacts becomes noticeable at upper atmospheric levels (Fig. 3b) with increase in time and energy flux. At time t= 2.92s (Fig. 3c) being close to the beam's maximum energy flux, the impacts produce polarisation comparable and higher than that from the external radiation. At a column depth of $2 \cdot 10^{20} cm^{-2}$, for instance, it reaches 5% and then sharply decreases with depth to 0.5-1%.

At a column depth of $1 \cdot 10^{21} cm^{-2}$ there is a secondary increase of polarisation, caused by beam electrons, that has the same magnitude about 2% as for the external radiation.

This increase can be explained by the beam kinetics owing to the return current effect that at the upper latmospheric evels causes a split of the initial beam into two beams moving downwards with separate maximums in energy distributions (Zharkova et al. 1995). At depth of $1 \cdot 10^{21} cm^{-2}$ the return current effect becomes negligible owing to the different reasons. These two beams merge again into a single directed beam with higher abundance of lower energy electrons appeared from Ohmic losses in addition to collisions. At this depth the electrons are responsible for increase in the H_α-line polarisation (Fig. 3) and intensity (Fig. 4).

When the beam reaches its maximum flux ($F_0 = 4 \cdot 10^{14} cm^{-2} s^{-1}$), at all levels impacts with beam electrons prevail over any other mechanisms including external radiation (Fig. 3d). For a viewing angle of $\pi/2$, at the injection site the polarisation reaches 25%, varying for other depths in a range of $15 - 20\%$ with a secondary increase at the same level $1 \cdot 10^{21} cm^{-2}$, as discussed above. Below this level the H_α-line polarisation falls to 2% which reflects the fact that the beam impacts become negligible, and polarisation is governed by the external chromospheric radiation.

The H_α-line impact polarisation is shown to be strongly affected by the viewing angle with a diversity of polarisation from 5% for $\theta = 0.1\pi$ to 20% for $\theta = 0.5\pi$ (see Fig. 3c-d). The bigger is the viewing angle the higher (in absolute value) is the negative polarisation, reaching its maximum at an angle of 90^o.

4.3. Interpretation of some observational features

Despite the fact that there are no H_α-line polarimetric observations available with high temporal resolution during the impulsive phase of flares when the current simulations are most applicable, an attempt is made to apply them to some observational features obtained during the first few minutes of a flare onset in the observations of Firstova & Boulatov (1996, thereafter FB). For comparison, the observations performed during the decay phase were also considered (Hénoux & Chambe 1990a; Hénoux et al. 1990b, thereafter HE).

The linear polarisation was found in about 30% of the observed H_α-spectra (FB). The absolute value of polarisation did not exceed 10% (HE), although in the observations of early phase of flare an average degree of polarisation was about 7% reaching 20% in the regions with weaker emission and in adjacent areas of the weakly perturbed chromosphere (FB). The H_α-line polarisation observed during the decay phase was positive in about 70% of observations with the plane of polarisation being parallel to the solar centre direction (HE). The plane of polarisation was close to the flare-to-solar centre direction for parts of a flare with higher emission whereas for weaker parts the plane of polarisation was perpendicular to this direction (FB).

Recently, an interpretation of the observed polarisation in H_α-line was attempted using the density matrix formalism for proton beams precipitating into a flaring atmosphere (Vogt et al. 1997). Collisions of hydrogen atoms with proton beams and the ambient plasma electrons were taken into account as well as the radiative transitions for incident and diffusive radiative fields in H_α, L_α and L_β frequencies. However, the calculated H_α-line polarisation was found to be lower by up to an order of magnitude than the one observed in flares, thereby, fitting the observations only for a very weak emission at the very beginning of a flare onset (Vogt et al. 1997). In order to fit the observations, other agents of H_α- line polarisation in flares have to be considered.

In the present paper, the impacts with beam electrons during their precipitation into a flaring atmosphere were considered as

a source of the H_α-line polarisation using the similar density matrix approach as it has been used for proton beams. The calculated magnitude of H_α-polarisation caused by these impacts with beam electrons varies from a few to 25% that is within the limits found in the observations. If hydrogen atoms can maintain a level of excitation and ionisation for a few minutes after the beam offset, for instance, because of lower recombination rates in comparison with the excitation and ionisation ones, then these figures for polarisation above can be valid during these few minutes and it can be observed in the early flash phase.

Another question is why for weaker parts of a flare polarisation is higher and for brighter parts lower. In the present study it was assumed that the H_α-line emission, originating in higher parts of the loop is likely to be less affected by beam electrons. It happens because they just started their precipitation from the top of the loop and at this depth the magnetic field is not high enough to give a strong splitting of atom levels into fine structure. However, this part of the loop could be the brightest one in the H_α emission owing to the number of neutral hydrogen atoms affected by beam electrons being high enough and their optical thickness being less than or about unity. Thus, H_α emission can escape completely from the volume that leads to observation of a higher intensity in emission. With further beam precipitation into the loop's feet themagnetic field increases as well as atom levels splitting into fine structure while the H_α-line optical opacity becomes much higher (Zharkova & Kobylinsky 1993; Kobylinsky & Zharkova 1996). This results in H_α radiation being trapped by radiative transfer effects and a lesser part of it being emitted while polarisation increases with depth owing to increasing Zeeman splitting.

The kinetics of beam precipitation into a flaring atmosphere (Sect. 2.2) can also explain why only 30% of flares expose linear polarisation. Only beams with a moderate intensity and spectral index can precipitate to the lower chromosphere as a directed beam, thereby, overcoming the effects of a return current at the transition region and the upper chromosphere. Very intense and hard beams are completely disrupted by this effect at the transition region whereas weak soft beams lose their energy in Coulomb collisions at the upper chromospheric levels. It is likely that 30% reflects the number of moderate intensity electron beams causing hydrogen emission and polarisation effects.

However, there is a key question to ask whether a calculated direction of plane of polarisation can meet the observational features of polarisation being positive in 70% of cases. The dependence of polarisation on a viewing angle seems to be rather important for the direction of polarisation (see Fig. 3 and Sect. 3.6 for the definitions) and it can be accounted for the plane of observed polarisation.

Beam electrons propagate along magnetic field lines which on top of the loop are nearly parallel to the solar surface and perpendicular to the observer looking from the top. This beam produces a higher intensity in the direction perpendicular to a beam propagation than in the parallel direction. Therefore, for the observer looking from the top, positive polarisation can be measured. On the other hand, in the loop's feet standing vertically, the direction of electron precipitation is parallel to the observer still looking from the top, and, hence, the resulting H_α-line polarisation is negative.

In real observations the observer can look onto the loop from the side or it can have inclinations to one or other side. Also, areas projected from the top of the loop on the horizontal plane are normally bigger by a factor 2/3 than those from the feet. Therefore, the fact that 70% of flares have positive polarisation in the observations by Firstova & Boulatov (1996) might indicate both a projection effect and a dominance of inclined loops in the observations.

However, these are speculations that need to be confirmed with observations with high spatial and temporal resolutions carried out during the impulsive and early flash phases of flares that, we believe, will become available in the future.

5. Conclusions

The H_α-line polarisation produced by electron beam impacts with Hydrogen atoms embedded into a flaring atmosphere with magnetic field was calculated using the density matrix approach.

The following conclusions are made:

1. In absence of electron beams the H_α-line linear polarisation is determined by the external chromospheric radiation starting from depth $1.2 \cdot 10^{21} cm^{-2}$ downwards to the photosphere and it reaches a magnitude about $2-3\%$.
2. The H_α-line profiles show a linear polarisation in a range of $-2-25\%$ only in the line cores where a 'weak magnetic field' approximation appears to be valid; the wings are fully depolarised by thermal collisions.
3. The circular polarisation is negligible.
4. On the top of atmosphere linear polarisation in the H_α-line profile is negative for the transitions with a bigger J being about $-10-15\%$ and positive for a smaller J reaching about 25%. From depth of $7 \cdot 10^{20} cm^{-2}$ the polarisation in all transition changes to a negative one being about $-2-10\%$ at the beginning of beam injection and decreasing to $-20-25\%$ at maximum of the beam flux.
5. The full H_α-line linear polarisation caused by impacts with beam electrons is negative varying from $-5-10\%$ to $-18-25\%$ for viewing angles $\theta = 0.1\pi$ and $\theta = \pi/2$, respectively.
6. The full H_α-line linear polarisation varies from $2-3\%$ in the upper chromosphere for the first seconds of electron beam injection to $10-25\%$ in the lower chromosphere for a maximum energy flux of the beam.
7. There is a secondary maximum of linear polarisation appearing in the lower chromosphere at a column depth of $1.0 \cdot 10^{21} cm^{-2}$. This is caused by an increasing abundance of low energy beam electrons precipitating downwards below the upper chromosphere where the return current electric field becomes negligible.

Accordingly, it has been shown that electron beams can be the agents producing some features observed in the H_α-line polarisation during the early phases (first few minutes) of solar flares. In order to discriminate the effects of electron beams from those

caused by proton beams, the complex multi-wavelength observations with high temporal and spectral resolution are required.

References

Aboudarham J., Hénoux J.C., 1986, A&A 168, 301
Aboudarham J., Hénoux J.C., 1987, A&A 174, 270
Berestetskii V.B., Liphshits E.M., Pitaevskij L.P., 1989, Quantum Electrodynamics. Nauka, Moscow, 728
Bommier V., 1980, A&A 87, 109
Bommier V., 1996, Solar.Phys 164, 29
Bommier V., Landi Degl'Innocenti E., 1996, Solar Phys. 164, 117
Bommier V., Landi Degl'Innocenti E., Sahal-Brechot S., 1991, A&A 244, 383
Bommier V., Landi Degl'Innocenti E., Sahal-Brechot S., 1996, Solar Phys. 164, 117
Chambe G., Hénoux J.C., 1979, A&A 80, 123
Emslie A.G., 1980, ApJ 235, 1055
Firstova N.M., Boulatov A.V., 1996, Solar Phys. 164, 361
Fletcher L., Brown J.C., 1995, A&A 294, 260
Hénoux J.C., Semel M., 1981, Solar Maximum Year 1, 207
Hénoux J.C., 1991, Solar Polarimetry. NSO/SP Summer Workshop Series. 11, 285
Hénoux J.C., Chambe G., 1990a, J. Quant. Spectrosc. Radiat. Transf. 44, 193
Hénoux J.C., Chambe G., Smith D., et al.,1990b, ApJS 73, 303
Hénoux J.C., Fang C., Gan W.Q., 1993, A&A 274, 923
Kobylinskij V.A.,.Zharkova V.V., 1996, Adv. Space Res. 17, N4-5, 110
Landi Degl'Innocenti E., 1982, Solar Phys. 79, 291
Landi Degl'Innocenti E., 1983, Solar Phys. 85, 33
Landi Degl'Innocenti E., 1985, Solar Phys. 102, 1
Landi Degl'Innocenti E., 1996, Solar Phys. 164, 21
Landi Degl'Innocenti E., Bommier V., Sahal-Brechot S., 1990, A&A 235, 459
Landi Degl'Innocenti E., Bommier V., Sahal-Brechot S., 1991a, A&A 244, 391
Landi Degl'Innocenti E., Bommier V., Sahal-Brechot S., 1991b, A&A 244, 401
Li P., Emslie A.G., Mariska J.T., 1989, ApJ 341, 1075
Lozitskii V.G., Baranovskij E.A., 1993, Bulletin of the Crimean Astrophysical Observatory 88, 58
Mariska J.T., Emslie A.G., Li P., 1989, ApJ 341, 1067
Silva A.V.R., White S.M., Lin R.P., et al., 1996, ApJS 106, 621
Somov B.V., Syrovatskii S.I., Spector A.R., 1981, Solar Phys. 73, 145
Syniavskii D.V., Zharkova V.V., 1994, ApJS 90, 729 (Paper I)
Vogt E., Hénoux J.C., 1996, Solar Phys. 164, 345
Vogt E., Sahal-Brechot S., Hénoux J.C., 1997, A&A 324, 1211
Voitenko Yu.M., 1998, Solar Phys. 182, 411
Zharkova V.V., Brown J.C., 1995, Proc.3rd SOHO Workshop Estes Park, Colorado, USA, ESA SP-373, 61
Zharkova V.V., Kobylinskii V.A., 1989, SvA Letters 15, 366
Zharkova V.V., Kobylinskii V.A., 1991, SvA Letters 17, 34
Zharkova V.V., Kobylinskii V.A., 1993, Solar Phys. 143, 259
Zharkova V.V., Brown J.C., Syniavskii D.V., 1995, A&A 304, 284 (Paper II)